Progress In Electromagnetics Research, Vol. 121, 505–520, 2011

PARALLEL IMPLEMENTATION OF MLFMA FOR HOMOGENEOUS OBJECTS WITH VARIOUS MATERIAL PROPERTIES

Ö. Ergül*

Department of Mathematics and Statistics, University of Strathclyde, Glasgow, UK

Abstract—We present a parallel implementation of the multilevel fast multipole algorithm (MLFMA) for fast and accurate solutions of electromagnetics problems involving homogeneous objects with diverse material properties. Problems are formulated rigorously with the electric and magnetic current combined-field integral equation (JMCFIE) and solved iteratively using MLFMA parallelized with the hierarchical partitioning strategy. Accuracy and efficiency of the resulting implementation are demonstrated on canonical problems involving perfectly conducting, lossless dielectric, lossy dielectric, and double-negative spheres.

1. INTRODUCTION

Real-life electromagnetics phenomena, such as scattering from airborne targets [1], radiation from antennas [2], transmission through dielectric lenses [3], metamaterials [4], and photonic crystals [5], often involve large objects with respect to wavelength. Accurate discretizations of these objects lead to large matrix equations, even when they are formulated with the surface integral equations. The resulting large-scale problems can be solved iteratively, where the required matrix-vector multiplications are performed efficiently with various acceleration methods, such as the fast Fourier transform (FFT) [6, 7], the adaptive integral method [8], and especially the multilevel fast multipole algorithm (MLFMA) [9–13], which has been successfully used to solve many challenging problems in various application areas [1–5, 14].

Received 25 September 2011, Accepted 26 October 2011, Scheduled 4 November 2011

* Corresponding author: Özgür Ergül (ozgur.ergul@strath.ac.uk).

For a problem involving $\mathcal{O}(N)$ unknowns, MLFMA provides each matrix-vector multiplication in $\mathcal{O}(N \log N)$ time using $\mathcal{O}(N \log N)$ memory. On the other hand, a sequential implementation of MLFMA running on a single processor may not be sufficient to solve very large problems discretized with millions of unknowns. In order to solve such extremely large problems, MLFMA can be parallelized on distributed-memory architectures [15–26]. Different strategies, such as the hybrid partitioning [15–18], asynchronous partitioning [19, 20], FFT-based methods [21–23], and hierarchical partitioning [24–26], have been developed for the efficient parallelization of MLFMA, increasing the problem size from tens of millions to hundreds of millions in the last decade. However, these studies have mainly focused on perfectly conducting objects, whereas less attention has been paid to penetrable objects.

In this work, we present a parallel implementation of MLFMA for homogeneous objects. Problems are formulated with the electric and magnetic current combined-field integral equation (JMCFIE) [27–29] and discretized with the Rao-Wilton-Glisson (RWG) functions [30] on triangular domains. MLFMA is parallelized using the hierarchical partitioning strategy, which provides efficient parallelization for penetrable and non-penetrable homogeneous objects [3, 24–26]. We show that the resulting rigorous implementation is capable of analyzing large-scale objects with diverse material properties, such as metallic, lossless dielectric, and lossy dielectric, as well as those with negative permittivity and permeability for the homogenization of metamaterials. Accuracy and efficiency of the implementation are demonstrated on canonical problems involving various types of spheres.

The rest of the paper is organized as follows. In Section 2, we present a compact formulation for the solution of electromagnetics problems using JMCFIE and MLFMA. Hierarchical parallelization is discussed in Section 3, including pseudocodes of major operations in parallel MLFMA. Section 4 includes a brief discussion on material properties, followed by numerical results in Section 5, and concluding remarks in Section 6.

2. SOLUTIONS WITH JMCFIE AND MLFMA

Consider electromagnetics problems involving time-harmonic fields with $e^{-i\omega t}$ time dependence. For numerical solutions, JMCFIE can be discretized with the RWG functions on triangular domains using a Galerkin scheme. The interaction of the mth testing function $\mathbf{t}_m$ ($m = 1, 2, \ldots, N$) and the nth basis function $\mathbf{b}_n$ ($n = 1, 2, \ldots, N$) through a homogeneous domain D_u with electrical parameters $\{\epsilon_u, \mu_u\}$

can be written as

$$\bar{\mathbf{Z}}_u^{(11)}[m,n] = \gamma_{u,n}\Big\{\alpha\gamma_{u,m}\bar{\mathbf{T}}_u^T[m,n] + (1-\alpha)\bar{\mathbf{K}}_{PV,u}^N[m,n] - \frac{1}{2}(1-\alpha)\gamma_{u,m}\bar{\mathbf{I}}^T[m,n]\Big\} = \bar{\mathbf{Z}}_u^{(22)}[m,n] \quad (1)$$

$$\bar{\mathbf{Z}}_u^{(12)}[m,n] = \gamma_{u,n}\eta_u^{-1}\Big\{(1-\alpha)\bar{\mathbf{T}}_u^N[m,n] - \alpha\gamma_{u,m}\bar{\mathbf{K}}_{PV,u}^T[m,n] - \frac{1}{2}\alpha\bar{\mathbf{I}}^N[m,n]\Big\} \quad (2)$$

$$\bar{\mathbf{Z}}_u^{(21)}[m,n] = -\eta_u^2\bar{\mathbf{Z}}_u^{(12)}[m,n], \quad (3)$$

where α is a combination parameter, $\gamma_{u,m} = \pm 1$ and $\gamma_{u,n} = \pm 1$ represent the orientations of the testing and basis functions, respectively, $\eta_u = \sqrt{\mu_u}/\sqrt{\epsilon_u}$ is the intrinsic impedance of the medium, and

$$\left\{\begin{array}{c}\bar{\mathbf{T}}_u^T\\ \bar{\mathbf{T}}_u^N\end{array}\right\}[m,n] = \int_{S_m}\left\{\begin{array}{c}\mathbf{t}_m(\mathbf{r})\\ \mathbf{t}_m(\mathbf{r})\times\hat{\mathbf{n}}(\mathbf{r})\end{array}\right\}\cdot\mathcal{T}_u\{\mathbf{b}_n\}(\mathbf{r}) \quad (4)$$

$$\left\{\begin{array}{c}\bar{\mathbf{K}}_{PV,u}^T\\ \bar{\mathbf{K}}_{PV,u}^N\end{array}\right\}[m,n] = \int_{S_m}\left\{\begin{array}{c}\mathbf{t}_m(\mathbf{r})\\ \mathbf{t}_m(\mathbf{r})\times\hat{\mathbf{n}}(\mathbf{r})\end{array}\right\}\cdot\mathcal{K}_{PV,u}\{\mathbf{b}_n\}(\mathbf{r}) \quad (5)$$

$$\left\{\begin{array}{c}\bar{\mathbf{I}}^T\\ \bar{\mathbf{I}}^N\end{array}\right\}[m,n] = \int_{S_m}\left\{\begin{array}{c}\mathbf{t}_m(\mathbf{r})\\ \mathbf{t}_m(\mathbf{r})\times\hat{\mathbf{n}}(\mathbf{r})\end{array}\right\}\cdot\mathbf{b}_n(\mathbf{r}) \quad (6)$$

are discretized operators. In (4)–(6), $\hat{\mathbf{n}}(\mathbf{r})$ is the oriented unit normal vector. The integro-differential operators are applied to the nth basis function as

$$\mathcal{T}_u\{\mathbf{b}_n\}(\mathbf{r}) = ik_u\int_{S_n}d\mathbf{r}'\mathbf{b}_n(\mathbf{r}')\left[\frac{\exp(ik_u|\mathbf{r}-\mathbf{r}'|)}{4\pi|\mathbf{r}-\mathbf{r}'|}\right] + \frac{i}{k_u}\int_{S_n}d\mathbf{r}'\nabla'\cdot\mathbf{b}_n(\mathbf{r}')\nabla\left[\frac{\exp(ik_u|\mathbf{r}-\mathbf{r}'|)}{4\pi|\mathbf{r}-\mathbf{r}'|}\right] \quad (7)$$

$$\mathcal{K}_{PV,u}\{\mathbf{b}_n\}(\mathbf{r}) = \int_{PV,S_n}d\mathbf{r}'\mathbf{b}_n(\mathbf{r}')\times\nabla'\left[\frac{\exp(ik_u|\mathbf{r}-\mathbf{r}'|)}{4\pi|\mathbf{r}-\mathbf{r}'|}\right], \quad (8)$$

where $k_u = \omega\sqrt{\epsilon_u}\sqrt{\mu_u} = 2\pi\lambda_u^{-1}$ is the wavenumber.

Consider an object with electrical parameters $\{\epsilon_i, \mu_i\}$ in a host domain $\{\epsilon_o, \mu_o\}$ extending to infinity. If the object is penetrable, a $2N \times 2N$ matrix equation can be derived, where the matrix elements involve contributions from the inner and outer media, i.e.,

$$\bar{\mathbf{Z}}^{(ab)}[m,n] = \bar{\mathbf{Z}}_i^{(ab)}[m,n] + \bar{\mathbf{Z}}_o^{(ab)}[m,n] \quad (9)$$

for $a = 1, 2$, $b = 1, 2$, $m = 1, 2, \ldots N$, and $n = 1, 2, \ldots N$. On the other hand, if the object is a perfect electric conductor (PEC), an $N \times N$ matrix equation with

$$\bar{\mathbf{Z}}^{(11)}[m,n] = \bar{\mathbf{Z}}_o^{(11)}[m,n] \tag{10}$$

is derived and solved to obtain the coefficients for the electric current, while the rest of the interactions are omitted. In this case, the resulting matrix equations are identical to those obtained with the combined-field integral equation (CFIE) [31].

In MLFMA, interactions are factorized as

$$\bar{\mathbf{Z}}_u^{(ab)}[m,n] \approx \int d^2\hat{\mathbf{k}} \mathbf{F}_{u,m}^{(ab)}(\mathbf{r}_C, \hat{\mathbf{k}}) \cdot \tau(\mathbf{r}_C - \mathbf{r}_{C'}, \hat{\mathbf{k}}) \mathbf{R}_{u,n}^{(ab)}(\mathbf{r}_{C'}, \hat{\mathbf{k}}), \tag{11}$$

where $\mathbf{F}_{u,m}^{(ab)}$ is the receiving pattern of the mth testing function, $\mathbf{R}_{u,n}^{(ab)}$ is the radiation pattern of the nth basis function, and $\tau(\mathbf{r}_C - \mathbf{r}_{C'}, \hat{\mathbf{k}})$ is a combination of shift and translation operators to transform the radiated field at $\mathbf{r}_{C'}$ into incoming field at $\mathbf{r}_C$. The radiation pattern does not depend on the interaction type, i.e.,

$$\begin{aligned} \mathbf{R}_{u,n}^{(11)}(\mathbf{r}_{C'}, \mathbf{k}_u) &= \mathbf{R}_{u,n}^{(12)}(\mathbf{r}_{C'}, \mathbf{k}_u) = \mathbf{R}_{u,n}^{(21)}(\mathbf{r}_{C'}, \mathbf{k}_u) = \mathbf{R}_{u,n}^{(22)}(\mathbf{r}_{C'}, \mathbf{k}_u) \\ &= \gamma_{u,n} \bar{\psi} \cdot \int_{S_n} d\mathbf{r}' \exp[-i\mathbf{k}_u \cdot (\mathbf{r}' - \mathbf{r}_{C'})] \mathbf{b}_n(\mathbf{r}'), \end{aligned} \tag{12}$$

where $\mathbf{k}_u = \hat{\mathbf{k}} k_u$, $\bar{\psi} = (\bar{\mathbf{I}}_{3\times 3} - \hat{\mathbf{k}}\hat{\mathbf{k}})$, and $\bar{\mathbf{I}}_{3\times 3}$ is the 3×3 unit dyad. On the other hand,

$$\mathbf{F}_{u,m}^{(11)}(\mathbf{r}_C, \mathbf{k}_u) = \alpha \gamma_{u,m} \mathbf{F}_{u,m}(\mathbf{r}_C, \mathbf{k}_u) + (1-\alpha) \mathbf{F}_{u,m}^{\times n \times k}(\mathbf{r}_C, \mathbf{k}_u) \tag{13}$$

$$= \mathbf{F}_{u,m}^{(22)}(\mathbf{r}_C, \mathbf{k}_u) \tag{14}$$

$$\mathbf{F}_{u,m}^{(12)}(\mathbf{r}_C, \mathbf{k}_u) = \eta_u^{-1} \Big\{ (1-\alpha) \mathbf{F}_{u,m}^{\times n}(\mathbf{r}_C, \mathbf{k}_u) - \alpha \gamma_{u,m} \mathbf{F}_{u,m}^{\times k}(\mathbf{r}_C, \mathbf{k}_u) \Big\} \tag{15}$$

$$\mathbf{F}_{u,m}^{(21)}(\mathbf{r}_C, \mathbf{k}_u) = -\eta_u^2 \mathbf{F}_{u,m}^{(12)}(\mathbf{r}_C, \mathbf{k}_u), \tag{16}$$

where

$$\mathbf{F}_{u,m}(\mathbf{r}_C, \mathbf{k}_u) = \bar{\boldsymbol{\psi}} \cdot \int_{S_n} d\mathbf{r} \exp[i\mathbf{k}_u \cdot (\mathbf{r} - \mathbf{r}_C)] \mathbf{t}_m(\mathbf{r}) \tag{17}$$

$$\mathbf{F}_{u,m}^{\times n}(\mathbf{r}_C, \mathbf{k}_u) = \bar{\boldsymbol{\psi}} \cdot \int_{S_n} d\mathbf{r} \exp[i\mathbf{k}_u \cdot (\mathbf{r} - \mathbf{r}_C)] \mathbf{t}_m(\mathbf{r}) \times \hat{\mathbf{n}}(\mathbf{r}) \tag{18}$$

$$\mathbf{F}_{u,m}^{\times k}(\mathbf{r}_C, \mathbf{k}_u) = \mathbf{F}_{u,m}(\mathbf{r}_C, \mathbf{k}_u) \times \hat{\mathbf{k}} \tag{19}$$

$$\mathbf{F}_{u,m}^{\times n \times k}(\mathbf{r}_C, \mathbf{k}_u) = \mathbf{F}_{u,m}^{\times n}(\mathbf{r}_C, \mathbf{k}_u) \times \hat{\mathbf{k}}. \tag{20}$$

For fast solutions, the patterns in (12) and (17)–(20) are calculated and stored in memory to be used multiple times during iterations.

3. HIERARCHICAL PARALLELIZATION

MLFMA can be parallelized efficiently using the hierarchical partitioning strategy, which is based on simultaneous partitioning of subdomains and field samples. Consider a tree structure of $L+2 = \mathcal{O}(\log N)$ levels. At levels $l = 1, 2, \ldots, L$, there are N_l subdomains and S_l field samples with $N_l S_l = \mathcal{O}(N)$ to compute the interactions in accordance with the factorization in (11). Let the tree structure be parallelized into P processes. At level l, process p is assigned to N_l^p subdomains and S_l^p samples with $N_l^p S_l^p = \mathcal{O}(N/p)$ via a load-balancing algorithm. Intermediate levels $l+1/2$ for $l = 1, 2, \ldots, L-1$ are defined to facilitate operations in the hierarchical strategy. Specifically, level $l + 1/2$ contains the subdomains (and their samples) at level $l + 1$, which are partitioned similar to those at level l [25].

Consider process p with a set of subdomains $\mathcal{N}_l^p$ and a set of samples $\mathcal{S}_l^p$ for $l = 1, 2, \ldots, L$ and $l + 1/2 = 3/2, 5/2, \ldots, L - 1/2$. Table 1 lists the major operations performed during an aggregation stage in process p to compute radiated fields of subdomains from the lowest level to the top of the tree structure. For each subdomain c_1 at an intermediate level $l + 1/2$, child subdomains in the same process are traced one by one. Given a child subdomain c_2, the local data are inflated via one-to-one communications. Then, the data are interpolated and divided into two parts according to the partitioning of the next level. After all subdomains at the intermediate level are considered, one-to-one communications are required to send the half of the stored data to a corresponding process and receive complementary data to change the partitioning.

Table 2 lists the major operations performed during a translation stage in process p. After all intra-process translations are performed, process p is paired with all other processes $p' \neq p$ for inter-process translations. Once a pairing is established, all levels are traced to transfer radiated fields from p' to p. The transferred field is converted into incoming fields for all subdomains in the far zone owned by p. Note that, for translations performed by p', radiated fields are transferred from p to p', before the pairing is disestablished.

Finally, Table 3 lists the major operations performed during a disaggregation stage in process p. As the reverse of the aggregation stage, subdomains are traced from level $l = L-1$ to $l = 1$. At each level, one-to-one communications are performed to change the partitioning for the intermediate level $l + 1/2$. Choosing a subdomain c_1 at this level, child subdomains at level l in the same process are traced one by one. Specifically, samples of the incoming field are anterpolated and deflated, exactly as the reverse of the inflation, via one-to-one communications. Also note that the resulting data are superposed

Table 1. Pseudocode of major operations performed in process p during an aggregation stage.

```
Do for each level l = 1, 2, ..., L − 1
  Do for each subdomain c1 ∈ N^p_{l+1/2} at level l + 1/2
    Do for each child subdomain c2 ⊂ c1 if c2 ∈ N^p_l
      • Inflations (one-to-one communications)
      • Interpolate and get S^p_l{c2 → c1}
    End
  End
  • One-to-one communications to change partitioning for l + 1
End
```

Table 2. Pseudocode of major operations performed in process p during a translation stage.

```
Do all intra-process translations
Do for each processor p' ≠ p if there exists translations
  Do for each level l = 1, 2, ..., L
    Do for each subdomain c1 ∈ N^{p'}_l involved in a translation
      • Receive S^{p'}_l{c1} from p'
      Do for each subdomain c2 ∈ N^p_l in the far-field list of c1
        • Compute S^p_l{c2 → c1} via translation
      End
    End
    Do for each subdomain c1 ∈ N^p_l involved in a translation
      • Send S^p_l{c1} to p'
    End
  End
End
```

with incoming fields due to translations to combine interactions at different levels.

4. MATERIAL PROPERTIES

This section presents how different materials are handled in the same implementation. Consider a homogeneous object with electrical parameters $\{\epsilon_i, \mu_i\}$, where $\epsilon_i = \epsilon_0\epsilon_{ir} + i\sigma_i/\omega$, located in a host domain $\{\epsilon_o, \mu_o\} = \{\epsilon_0, \mu_0\}$ (free space) that extends to infinity.

Table 3. Pseudocode of major operations performed in process p during a disaggregation stage.

Do for each level $l = L-1, L-2, \ldots, 1$
- One-to-one communications to change partitioning for $l + 1/2$

Do for each subdomain $c_1 \in \mathcal{N}^p_{l+1/2}$ at level $l + 1/2$

Do for each child subdomain $c_2 \subset c_1$ if $c_2 \in \mathcal{N}^p_l$
- Anterpolate and get $\mathcal{S}^p_l\{c_1 \to c_2\}$
- Deflations (one-to-one communications)

End

End

End

4.1. Perfect Electric Conductor

If the object is PEC, i.e., $\sigma_i \to \infty$, the matrix equation in (10) is formed. Only one tree structure is constructed for the outer medium, which can be parallelized efficiently using the hierarchical strategy [25]. The size of the subdomains at the lowest level is approximately $0.25\lambda_0$. The total number of samples at level l is determined by the refined excess bandwidth formula [14], i.e., $S_l \propto (k_0 d_l)^2$, where d_l is the size of subdomains.

4.2. Lossless Dielectric

If the object is lossless, i.e., $\sigma_i = 0$, a $2N \times 2N$ matrix equation with partitions as defined in (9) is formed. Two different tree structures are constructed, considering the inner and outer media, since the cluster size and the number of samples for radiated and incoming fields depend on the medium parameters. Each tree structure is parallelized separately using the hierarchical strategy [3]. Compared to the PEC case, the time per iteration is increased around eight-fold (two $N \times N$ multiplications are required for each partition). Besides, the matrix-vector multiplication time tends to increase as the permittivity or permeability of the object increases, since $S_l \propto (k_i d_l)^2 = \epsilon_i \mu_i (\omega d_l)^2$ for the inner tree structure. High contrast also has an adverse effect on the iterative convergence, as discussed in [32].

4.3. Lossy Dielectric

Similar to the lossless case, a $2N \times 2N$ matrix equations is derived when the object is lossy, i.e., $\sigma_i > 0$. Matrix partitions become diagonally

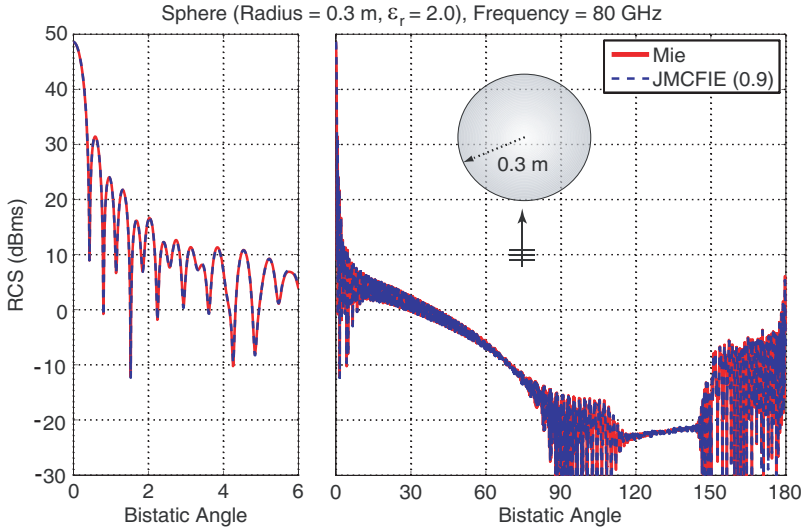

Figure 1. Solution of a scattering problem involving a lossless dielectric sphere of radius 0.3 m at 80 GHz in free space. The relative permittivity of the sphere is 2.0. RCS (in dBms) is plotted as a function of the bistatic angle, where 0° and 180° correspond to the forward-scattering and backscattering directions, respectively.

dominant as the conductivity increases, which may lead to better conditioned matrix equations that are easier to solve iteratively [33]. To determine the number of samples for the inner medium, we use $S_l \propto (|k_i|d_l)^2$ by inserting the absolute value of the wavenumber into the excess bandwidth formula.

4.4. Negative Parameters

JMCFIE is applicable to those objects with negative permittivity and/or permeability for the homogenization of metamaterials, provided that the roots when finding the wavenumber and intrinsic impedance are selected carefully [34]. In free space, negative parameters lead to a high-contrast object, whose iterative solution can be again challenging, especially if the object is lossless. The number of samples are determined by taking the absolute value of the wavenumber, i.e., $S_l \propto (|k_i|d_l)^2$.

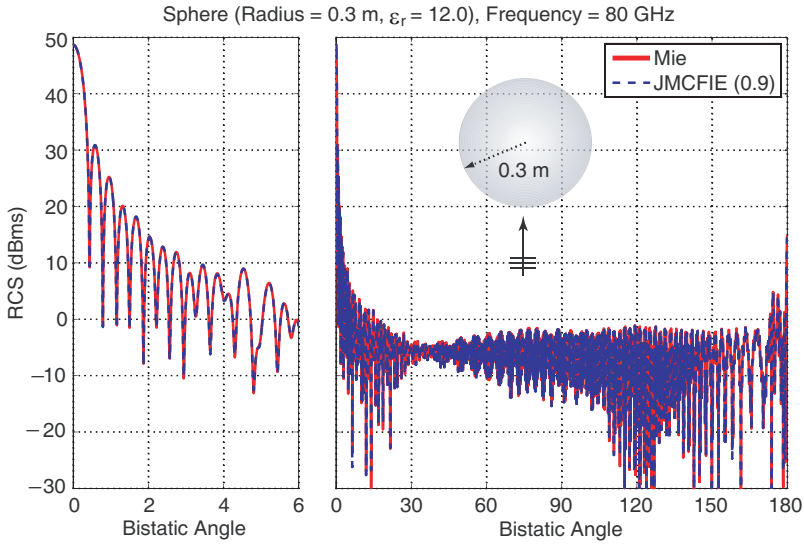

Figure 2. Solution of a scattering problem involving a lossless dielectric sphere of radius 0.3 m at 80 GHz in free space. The relative permittivity of the sphere is 12.0. RCS (in dBms) is plotted as a function of the bistatic angle, where 0° and 180° correspond to the forward-scattering and backscattering directions, respectively.

5. NUMERICAL EXAMPLES

As numerical examples, solutions of scattering problems involving a sphere of radius 0.3 m are presented. The sphere is located in free space and illuminated by a plane wave propagating in the z direction with the electric field polarized in the x direction at 80 GHz. Five different cases are considered:

- Lossless sphere with a relative permittivity of 2.0.
- High-contrast lossless sphere with a relative permittivity of 12.0.
- Lossy sphere with a relative permittivity of 2.0 and a conductivity of 1.0 S/m.
- PEC sphere.
- Double-negative sphere with a relative permittivity of -2.0 and a relative permeability of -1.6.

All problems are formulated with JMCFIE using $\alpha = 0.9$. This choice of the combination parameter is determined via numerical experiments and it seems to be suitable especially if high accuracy is desired using

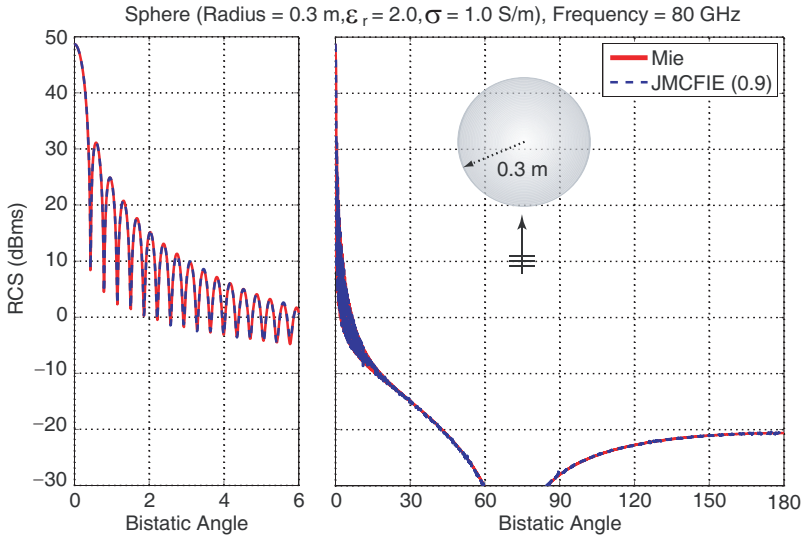

Figure 3. Solution of a scattering problem involving a lossy dielectric sphere of radius 0.3 m at 80 GHz in free space. The relative permittivity and conductivity of the sphere are 2.0 and 1.0 S/m, respectively. RCS (in dBms) is plotted as a function of the bistatic angle, where 0° and 180° correspond to the forward-scattering and backscattering directions, respectively.

the RWG functions. Discretizations with the RWG functions on $\lambda_0/10$ triangles lead to matrix equations involving 46,811,328 unknowns when the sphere is penetrable and 23,405,664 unknowns when the sphere is PEC. Problems are solved with MLFMA on a cluster of Intel Xeon Nehalem quad-core processors with 2.80 GHz clock rate. Using the hierarchical strategy, MLFMA is parallelized into 64 processes. Both near-zone and far-zone interactions are calculated with maximum 1% error. Iterative solutions are performed by the biconjugate-gradient-stabilized (BiCGStab) algorithm [35] without preconditioning. The target residual error for the convergence is selected as 0.005. For these accuracy parameters and the given model of processors, the parallelization efficiency is around 85% leading to 54-fold speedup using 64 processes compared to the corresponding sequential solution [3, 25]. Note that problems involving more complicated objects may require effective preconditioners, such as those based on the Schur-complement reduction for penetrable objects [5] and the two-level scheme for PEC objects [36] that are appropriate for MLFMA implementations.

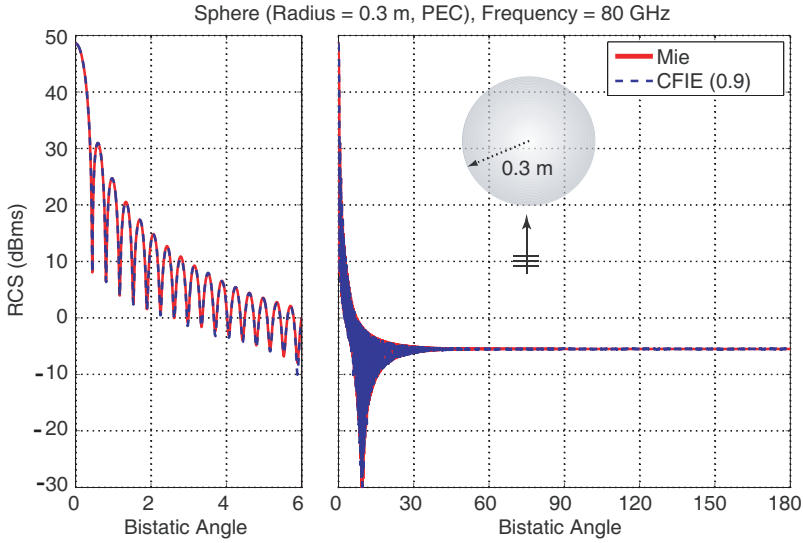

Figure 4. Solution of a scattering problem involving a PEC sphere of radius 0.3 m at 80 GHz in free space. RCS (in dBms) is plotted as a function of the bistatic angle, where 0° and 180° correspond to the forward-scattering and backscattering directions, respectively.

Figures 1–5 present the bistatic radar cross section (RCS) values (in dBms) on the z–x plane as a function of the bistatic angle θ from 0° to 180°, where 0° and 180° correspond to the forward-scattering and backscattering directions, respectively. RCS values around the forward-scattering direction are also focused in separate plots. Computational values obtained by using the parallel MLFMA are compared with those obtained via analytical Mie-series solutions. It can be observed that the computational values agree very well with the analytical results for all cases.

For more quantitative assessment of the accuracy and efficiency, Table 4 lists the number of iterations, total time (that is dominated by iterations), memory, and root-mean-square (RMS) error in computational values with respect to analytical values for the sphere problems. The fastest convergence is observed when the sphere is lossy, as a result of the improved conditioning for moderate values of conductivity. On the other hand, the convergence is significantly slower for high contrasts, e.g., for the lossless sphere with 12.0 permittivity and the double-negative sphere, as commonly observed in numerical solutions of JMCFIE [32]. As also expected, the fastest solution in terms of the processing time is obtained for the PEC case. The

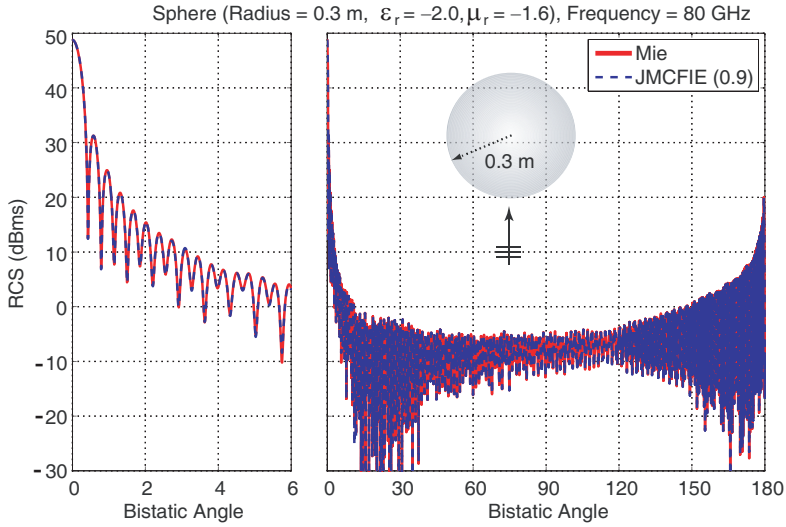

Figure 5. Solution of a scattering problem involving a double-negative sphere of radius 0.3 m at 80 GHz in free space. The relative permittivity and permeability of the sphere are -2.0 and -1.6, respectively. RCS (in dBms) is plotted as a function of the bistatic angle, where 0° and 180° correspond to the forward-scattering and backscattering directions, respectively.

Table 4. Solutions of scattering problems involving a sphere of radius 0.3 m at 80 GHz.

Electrical Parameters	Number of Iterations	Time (hours)	Memory (GB)	RMS Error
$\epsilon_r = 2.0$	143	31.2	387	0.36%
$\epsilon_r = 12.0$	178	88.6	714	0.91%
$\epsilon_r = 2.0$ & $\sigma = 1.0\,\mathrm{S/m}$	37	14.4	656	0.17%
PEC	125	3.33	155	0.21%
$\epsilon_r = -2.0$ & $\mu_r = -1.6$	198	48.1	415	0.23%

total time is generally proportional to the number of iterations, but it is remarkable that, in penetrable cases, the computing time also increases as the absolute values of the relative permittivity and permeability increase. For example, the high-contrast problem with relative permittivity of 12.0 requires 178 iterations and 88.6 hours, whereas it takes only 31.2 hours for 143 iterations when the relative

permittivity is 2.0. Finally, in all solutions listed in Table 4, the RMS error is below 1%, which is the target accuracy in our simulations. The highest error of 0.91% is obtained when the relative permittivity is 12.0, due to the sensitivity to geometric discretization for high contrasts.

6. CONCLUSION

A parallel implementation for large-scale objects discretized with millions of unknowns is presented. Problems involving homogeneous objects with various material properties are analyzed rigorously with the developed implementation based on a combination of JMCFIE, MLFMA, and the hierarchical partitioning strategy. Accuracy and efficiency of the implementation are demonstrated on very large scattering problems involving the sphere.

ACKNOWLEDGMENT

This work was supported by the Centre for Numerical Algorithms and Intelligent Software (EPSRC-EP/G036136/1) and by the Engineering and Physical Sciences Research Council (EPSRC) under Research Grant EP/J007471/1.

REFERENCES

1. Gürel, L., H. Bağci, J. C. Castelli, A. Cheraly, and F. Tardivel, "Validation through comparison: Measurement and calculation of the bistatic radar cross section (BRCS) of a stealth target," *Radio Sci.*, Vol. 38, No. 3, Jun. 2003.
2. Taboada, J. M., J. Rivero, F. Obelleiro, M. G. Araujo, and L. Landesa, "Method-of-moments formulation for the analysis of plasmonic nano-optical antennas," *J. Opt. Soc. Am. A*, Vol. 28, No. 7, 1341–1348, Jun. 2011.
3. Ergül, Ö., "Solutions of large-scale dielectric problems with the parallel multilevel fast multipole algorithm," *J. Opt. Soc. Am. A*, Vol. 28, No. 11, 2261–2268, Nov. 2011.
4. Gürel, L., Ö. Ergül, A. Ünal, and T. Malas, "Fast and accurate analysis of large metamaterial structures using the multilevel fast multipole algorithm," *Progress In Electromagnetics Research*, Vol. 95, 179–198, 2009.
5. Ergül, Ö., T. Malas, and L. Gürel, "Analysis of dielectric photonic-crystal problems with MLFMA and schur-complement

preconditioners," *J. Lightwave Technol.*, Vol. 29, No. 6, 888–897, Mar. 2011.

6. Gan, H. and W. C. Chew, "A discrete BCG-FFT algorithm for solving 3-D inhomogeneous scatterer problems," *Journal of Electromagnetic Waves and Applications*, Vol. 9, No. 10, 1339–1357, 1995.
7. Yuan, N., T. S. Yeo, X. C. Nie, L. W. Li, and Y. B. Gan, "Analysis of scattering from composite conducting and dielectric targets using the precorrected-FFT algorithm," *Journal of Electromagnetic Waves and Applications*, Vol. 17, No. 3, 499–515, 2003.
8. Bleszynski, E., M. Bleszynski, and T. Jaroszewicz, "AIM: Adaptive integral method for solving large-scale electromagnetic scattering and radiation problems," *Radio Sci.*, Vol. 31, No. 5, 1225–1251, 1996.
9. Song, J., C.-C. Lu, and W. C. Chew, "Multilevel fast multipole algorithm for electromagnetic scattering by large complex objects," *IEEE Trans. Antennas Propag.*, Vol. 45, No. 10, 1488–1493, Oct. 1997.
10. Sheng, X.-Q., J.-M. Jin, J. Song, W. C. Chew, and C.-C. Lu, "Solution of combined-field integral equation using multilevel fast multipole algorithm for scattering by homogeneous bodies," *IEEE Trans. Antennas Propag.*, Vol. 46, No. 11, 1718–1726, Nov. 1998.
11. Peng, Z., X.-Q. Sheng, and F. Yin, "An efficient twofold iterative algorithm of Fe-Bi-MLFMA using multilevel inverse-based ilu preconditioning," *Progress In Electromagnetics Research*, Vol. 93, 369–384, 2009.
12. Islam, S., J. Stiens, G. Poesen, R. Vounckx, J. Peeters, I. Bogaert, D. De Zutter, and W. De Raedt, "Simulation and experimental verification of W-band finite frequency selective surfaces on infinite background with 3D full wave solver NSPWMLFMA," *Progress In Electromagnetics Research*, Vol. 101, 189–202, 2010.
13. Yang, M.-L. and X.-Q. Sheng, "Parallel high-order Fe-Bi-MLFMA for scattering by large and deep coated cavities loaded with obstacles," *Journal of Electromagnetic Waves and Applications*, Vol. 23, No. 13, 1813–1823, 2009.
14. Chew, W. C., J.-M. Jin, E. Michielssen, and J. Song, *Fast and Efficient Algorithms in Computational Electromagnetics*, Artech House, Boston, MA, 2001.
15. Velamparambil, S., W. C. Chew, and J. Song, "10 million unknowns: Is it that big?" *IEEE Antennas Propag. Mag.*, Vol. 45, No. 2, 43–58, Apr. 2003.

16. Gürel, L. and Ö. Ergül, "Fast and accurate solutions of extremely large integral-equation formulations discretised with tens of millions of unknowns," *Electron. Lett.*, Vol. 43, No. 9, 499–500, Apr. 2007.
17. Pan, X.-M. and X.-Q. Sheng, "A sophisticated parallel MLFMA for scattering by extremely large targets," *IEEE Antennas Propag. Mag.*, Vol. 50, No. 3, 129–138, Jun. 2008.
18. Ergül, Ö. and L. Gürel, "Efficient parallelization of the multilevel fast multipole algorithm for the solution of large-scale scattering problems," *IEEE Trans. Antennas Propag.*, Vol. 56, No. 8, 2335–2345, Aug. 2008.
19. Fostier, J. and F. Olyslager, "An asynchronous parallel MLFMA for scattering at multiple dielectric objects," *IEEE Trans. Antennas Propag.*, Vol. 56, No. 8, 2346–2355, Aug. 2008.
20. Fostier, J. and F. Olyslager, "Full-wave electromagnetic scattering at extremely large 2-D objects," *Electron. Lett.*, Vol. 45, No. 5, 245–246, Feb. 2009.
21. Taboada, J. M., L. Landesa, F. Obelleiro, J. L. Rodriguez, J. M. Bertolo, M. G. Araujo, J. C. Mourino, and A. Gomez, "High scalability FMM-FFT electromagnetic solver for supercomputer systems," *IEEE Antennas Propag. Mag.*, Vol. 51, No. 6, 21–28, Dec. 2009.
22. Araujo, M. G., J. M. Taboada, F. Obelleiro, J. M. Bertolo, L. Landesa, J. Rivero, and J. L. Rodriguez, "Supercomputer aware approach for the solution of challenging electromagnetic problems," *Progress In Electromagnetics Research*, Vol. 101, 241–256, 2010.
23. Taboada, J. M., M. G. Araujo, J. M. Bertolo, L. Landesa, F. Obelleiro, and J. L. Rodriguez, "MLFMA-FFT parallel algorithm for the solution of large-scale problems in electromagnetics," *Progress In Electromagnetics Research*, Vol. 105, 15–30, 2010.
24. Ergül, Ö. and L. Gürel, "Hierarchical parallelisation strategy for multilevel fast multipole algorithm in computational electromagnetics," *Electron. Lett.*, Vol. 44, No. 1, 3–5, Jan. 2008.
25. Ergül, Ö. and L. Gürel, "A hierarchical partitioning strategy for efficient parallelization of the multilevel fast multipole algorithm," *IEEE Trans. Antennas Propagat.*, Vol. 57, No. 6, 1740–1750, Jun. 2009.
26. Ergül, Ö. and L. Gürel, "Rigorous solutions of electromagnetic problems involving hundreds of millions of unknowns," *IEEE Antennas Propag. Mag.*, Vol. 53, No. 1, 18–26, Feb. 2011.

27. Ylä-Oijala, P. and M. Taskinen, "Application of combined field integral equation for electromagnetic scattering by dielectric and composite objects," *IEEE Trans. Antennas Propagat.*, Vol. 53, No. 3, 1168–1173, Mar. 2005.
28. Ylä-Oijala, P., "Numerical analysis of combined field integral equation formulations for electromagnetic scattering by dielectric and composite objects," *Progress In Electromagnetics Research C*, Vol. 3, 19–43, 2008.
29. Ergül, Ö. and L. Gürel, "Efficient solution of the electric and magnetic current combined-field integral equation with the multilevel fast multipole algorithm and block-diagonal preconditioning," *Radio Sci.*, Vol. 44, No. 6001, Nov. 2009.
30. Rao, S. M., D. R. Wilton, and A. W. Glisson, "Electromagnetic scattering by surfaces of arbitrary shape," *IEEE Trans. Antennas Propagat.*, Vol. 30, No. 3, 409–418, May 1982.
31. Mautz, J. R. and R. F. Harrington, "*H*-field, *E*-field, and combined field solutions for conducting bodies of revolution," *AEÜ*, Vol. 32, No. 4, 157–164, Apr. 1978.
32. Ergül, Ö. and L. Gürel, "Comparison of integral-equation formulations for the fast and accurate solution of scattering problems involving dielectric objects with the multilevel fast multipole algorithm," *IEEE Trans. Antennas Propag.*, Vol. 57, No. 1, 176–187, Jan. 2009.
33. Ergül, Ö., "Fast and accurate solutions of electromagnetics problems involving lossy dielectric objects with the multilevel fast multipole algorithm," *Eng. Anal. Bound. Elem.*, Vol. 36, 423–432, 2012.
34. Rivero, J., J. M. Taboada, L. Landesa, F. Obelleiro, and I. Garcia-Tunon, "Surface integral equation formulation for the analysis of left-handed metamaterials," *Opt. Express*, Vol. 18, No. 15, 15876–15886, 2010.
35. Van Der Vorst, H. A., "Bi-CGSTAB: A fast and smoothly converging variant of Bi-CG for the solution of nonsymmetric linear systems," *SIAM J. Sci. Stat. Comput.*, Vol. 13, No. 2, 631–644, Mar. 1992.
36. Ergül, Ö., T. Malas, and L. Gürel, "Solutions of large-scale electromagnetics problems using an iterative inner-outer scheme with ordinary and approximate multilevel fast multipole algorithms," *Progress In Electromagnetics Research*, Vol. 106, 203–223, 2010.